VOL. 314 NOVEMBER, 2014 NO. 9

ESTABLISHED IN 1818 BY BENJAMIN SILLIMAN

American Journal of Science

AN INTERNATIONAL EARTH SCIENCE JOURNAL

C. Page Chamberlain and Danny M. Rye
EDITORS

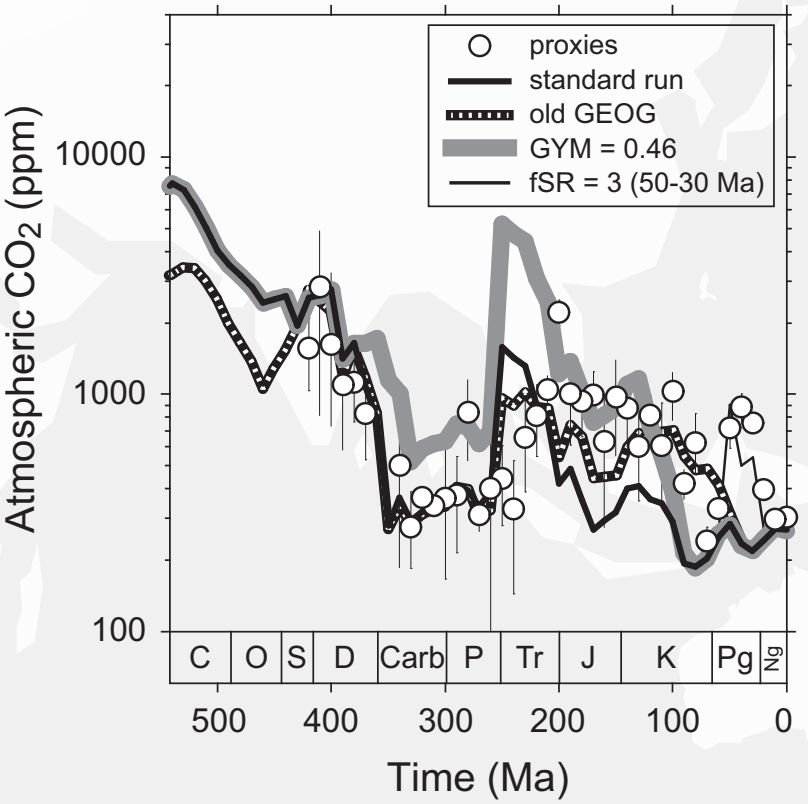

AMERICAN JOURNAL OF SCIENCE
KLINE GEOLOGY LABORATORY
YALE UNIVERSITY
NEW HAVEN, CONNECTICUT
AJSCAP 314(09) 1259-1372(2014)

[American Journal of Science, Vol. 314, November, 2014, P. 1259–1283, DOI 10.2475/09.2014.01]

American Journal of Science

NOVEMBER 2014

ERROR ANALYSIS OF CO_2 AND O_2 ESTIMATES FROM THE LONG-TERM GEOCHEMICAL MODEL GEOCARBSULF

DANA L. ROYER*,† YANNICK DONNADIEU**, JEFFREY PARK***, JENNIFER KOWALCZYK*, and YVES GODDÉRIS§

ABSTRACT. Long-term carbon and sulfur cycle models have helped shape our understanding of the Phanerozoic history of atmospheric CO_2 and O_2, but error analyses have been largely limited to testing only a subset of input parameters singly. As a result, the full ranges of probable CO_2 and O_2 are not quantitatively known. Here we investigate how variation in all 68 input parameters of the GEOCARBSULF model, both singly and in combination, affect estimated CO_2 and O_2. We improve formulations for land area, runoff, and continental temperature, the latter of which now excludes land area not experiencing chemical weathering. We find our resampled model CO_2 and O_2 estimates are well bounded and provide high confidence for a "double-hump" in CO_2 during the Phanerozoic, with high values during the early Paleozoic and Mesozoic, and low values during the late Paleozoic and late Mesozoic-to-Cenozoic. Our analyses also support a distinct atmospheric O_2 peak during the late Paleozoic (>30%) followed by low values near the Triassic-Jurassic boundary (~10%). Most of the spread in CO_2 is contributed by three factors: climate sensitivity to CO_2-doubling and the plant-assisted chemical weathering factors *LIFE* and *GYM*. CO_2 estimates during the Paleozoic to early Mesozoic are highly concordant with independent records from proxies, but are offset to lower values during the globally warm late Mesozoic to early Cenozoic. The model-proxy mismatch for the late Mesozoic can be eliminated with a change in *GYM* within its plausible range, but no change within plausible ranges can resolve the early Cenozoic mismatch. Either the true value for one or more input parameters during this interval is outside our sampled range, or the model is missing one or more key processes.

Key words: Carbon cycle, paleoclimate, models, carbon dioxide, oxygen, Phanerozoic

INTRODUCTION

Long-term carbon and sulfur cycle models for estimating atmospheric CO_2 and O_2 have provided many key insights into the operation of the ancient Earth system. Some highlights include the identification of a positive coupling between multi-million-year patterns of atmospheric CO_2 and temperature (Berner and others, 1983; Berner, 1990), evaluation of the importance of plant evolution on CO_2 levels (Berner, 1997), resolution of an atmospheric O_2 spike during the Carboniferous and Permian that is coincident with a period of insect gigantism (Berner and others, 2003), and, in concert with a general-circulation model (GCM), spatial quantification of chemical weathering rates through time and its impact on CO_2 (Gibbs and others, 1999; Goddéris and others, 2012, 2014).

* Department of Earth and Environmental Sciences, Wesleyan University, Middletown, Connecticut 06459, USA
** LSCE, IPSL, CEA-CNRS-UVSQ, Gif-sur-Yvette, France
*** Department of Geology and Geophysics, Yale University, New Haven, Connecticut 06511, USA
§ Géosciences Environnement Toulouse, CNRS-Université Paul Sabatier, Toulouse, France
† Corresponding author: droyer@wesleyan.edu

A popular long-term carbon and sulfur cycle model is GEOCARBSULF (Berner, 2006a). This model estimates atmospheric CO_2 and O_2 levels by reconstructing the important long-term sources and sinks through time, each of which is a function of multiple terms that can be estimated from the geologic record (Berner, 2004; see also METHODS). For example, the chemical weathering of calcium- and magnesium-rich silicate rocks, a critical sink for atmospheric CO_2 on geologic timescales (Walker and others, 1981; Berner and others, 1983), is dependent in part on climate, vegetation cover, lithology, and relief.

Confidence in estimates of atmospheric CO_2 and O_2 from GEOCARBSULF would improve by knowing how stable its predictions are to changes in its 68 input parameters. These parameters are either time-dependent (for example, seafloor-spreading rates) or assumed to be time-invariant (for example, activation energy for silicate mineral dissolution). Historically, the sensitivity of each time-dependent array on estimated CO_2 and O_2 was assessed by comparing a standard model run with one where the variable remains fixed at its present-day value, and the sensitivity of time-invariant constants was quantified by running the model with several value choices across likely ranges (for example, Berner, 2004). More recently, Royer and others (2007) and Park and Royer (2011) explored GEOCARBSULF's sensitivity to five constants using Monte Carlo simulations, both singly and in combination (*ACT*, *LIFE*, *GYM*, *FERT*, and ΔT_{2X}; see METHODS for definitions), to estimate a Bayesian probability density function (PDF) for climate sensitivity. For the most part, however, the combined effect of variance in the input parameters on estimated CO_2 and O_2 has been gauged qualitatively by expert knowledge; these error envelopes have been hand-drawn on figures and considered "best guesses" (for example, Berner and Kothavala, 2001).

Our study has two primary aims. First, we incorporate into GEOCARBSULF improved estimates of land area, runoff, and continental temperature from the coupled GCM-carbon cycle model of Goddéris and others (2012, 2014). Because their model resolves the spatial distribution of chemical weathering, continental areas with scant chemical weathering can be excluded (for example, deserts). This improvement has been suggested previously (Berner and Kothavala, 2001; Berner, 2004) but never before implemented. The second goal is to better quantify the range of probable CO_2 and O_2 from GEOCARBSULF. Our general strategy is to use Monte Carlo simulations to produce more realistic distributions of estimated CO_2 and O_2 based on variance in all 68 input parameters both singly and in combination. These calculations should improve our understanding of the long-term Earth system in two ways. First, they provide the best constraints yet on the stability of CO_2 and O_2 estimates over the Phanerozoic from GEOCARBSULF. This is especially true given that the last published CO_2 error envelope is for an outdated version (GEOCARB III; Berner and Kothavala, 2001). Second, our analyses may help identify variables that, owing to their current state of knowledge, lead to the greatest range in estimated CO_2 and O_2. This may be particularly important for the time-dependent variables, whose sensitivity was previously assessed in a rather simple way. Apart from a discussion related to the revised parameters from Goddéris and others (2012, 2014), we do not seek to identify the underlying processes that drive the CO_2 and O_2 patterns; the interested reader should consult Berner (2004).

METHODS

Overview of GEOCARBSULF Model

GEOCARBSULF tracks the multi-million-year transfer of carbon and sulfur between surface reservoirs (atmosphere, ocean, soil, living biomass) and rock reservoirs, principally reduced organic carbon, oxidized carbonate carbon, reduced pyrite sulfur,

and oxidized sulfate sulfur. Because the timescale of integration is sufficiently long in GEOCARBSULF (typically 10 m.y.), we assume that the surface reservoirs are in quasi-steady-state (Berner, 2004).

Important processes for transferring surface carbon to rock reservoirs include the burial of organic carbon and the chemical weathering of Ca-Mg silicate rocks to produce HCO_3^-, Ca^{2+}, and Mg^{2+} that precipitates and accumulates as carbonate rock. Carbon returns to the surface system via the weathering of sedimentary organic carbon and the degassing of organic and inorganic carbon from volcanism, metamorphism, and diagenesis (Ebelmen, 1845; Urey, 1952; Berner and Maasch, 1996; Berner, 2004). A simple mass balance tracks changes in carbon over time in the surface system. Also, because $\delta^{13}C$ values differ between the carbonate and organic carbon reservoirs, an isotopic mass balance provides additional constraints (Berner, 1991, 2004):

$$dM_c/dt = F_{wc} + F_{wg} + F_{mc} + F_{mg} - F_{bc} - F_{bg} \quad (1)$$

$$d(\delta_c M_c)/dt = \delta_{wc}F_{wc} + \delta_{wg}F_{wg} + \delta_{mc}F_{mc} + \delta_{mg}F_{mg} - \delta_{bc}F_{bc} - \delta_{bg}F_{bg} \quad (2)$$

where M_c = mass of carbon in surface system. The $\delta = \delta^{13}C$ isotopic factors and F = flux variables have subscripts *wc* = weathering of Ca and Mg carbonates, *wg* = weathering of sedimentary organic carbon, *mc* = degassing from carbonates, *mg* = degassing from organic carbon, *bc* = burial of carbonate, and *bg* = burial of organic carbon.

A similar set of processes describes the long-term cycling of sulfur, namely the burial, weathering, and degassing of sulfate sulfur and pyrite sulfur. Similar to equations (1-2), a pair of mass balance and isotopic mass balance equations tracks the cycling of reduced and oxidized sulfur. The long-term sulfur cycle primarily affects atmospheric O_2, not CO_2. By coupling the two cycles, atmospheric CO_2 and O_2 can be solved simultaneously.

The original GEOCARB model (Berner, 1990, 1991) has been updated multiple times, resulting in GEOCARB II (Berner, 1994), GEOCARB III (Berner and Kothavala, 2001), GEOCARBSULF (Berner, 2006a), and GEOCARBSULFvolc (Berner, 2006b, 2008). These updates involve either improvements to or the addition of factors for constraining one of the fluxes in equations (1-2) or the equivalent equations for sulfur. For example, in GEOCARB III results from a GCM were introduced to parameterize the dependence of global-mean surface temperature and runoff on CO_2. Our study uses the newest version of the carbon-cycle model, GEOCARBSULFvolc (Berner, 2006b, 2008); for convenience, we refer to the model as GEOCARBSULF.

Parameters Considered in Study: Time Series

We describe here the twelve time-dependent parameters in GEOCARBSULF (see also Appendix 1 and fig. 1). Each parameter is expressed within the model as a time series over the Phanerozoic with 10-m.y. sampling and is calibrated to the Gradstein and others (2004) timescale.

Isotope time series ($^{87}Sr/^{86}Sr$, $\delta^{13}C$, and $\delta^{34}S$).—The $^{87}Sr/^{86}Sr$ of shallow marine carbonate is sensitive to the global fraction of volcanic (vs. non-volcanic) rock weathering (see discussion in next section). The $\delta^{13}C$ of shallow marine carbonate and $\delta^{34}S$ of $CaSO_4$ sulfur help track the burial flux of organic matter and pyrite. Prokoph and others (2008) provide composite time series for these three isotopic quantities. For $\delta^{34}S$ and especially $\delta^{13}C$, random deviations lead to model failure during the early Paleozoic so frequently that model sensitivities were difficult to estimate (we describe our criteria for model failure in the section "The Code and Resampling Strategy"). For the strontium ratio and $\delta^{13}C$, we therefore retain the standard GEOCARBSULF time series (figs. 1A-1B) (Berner, 2004, 2006a, 2009). Even for our adopted $\delta^{13}C$ time series,

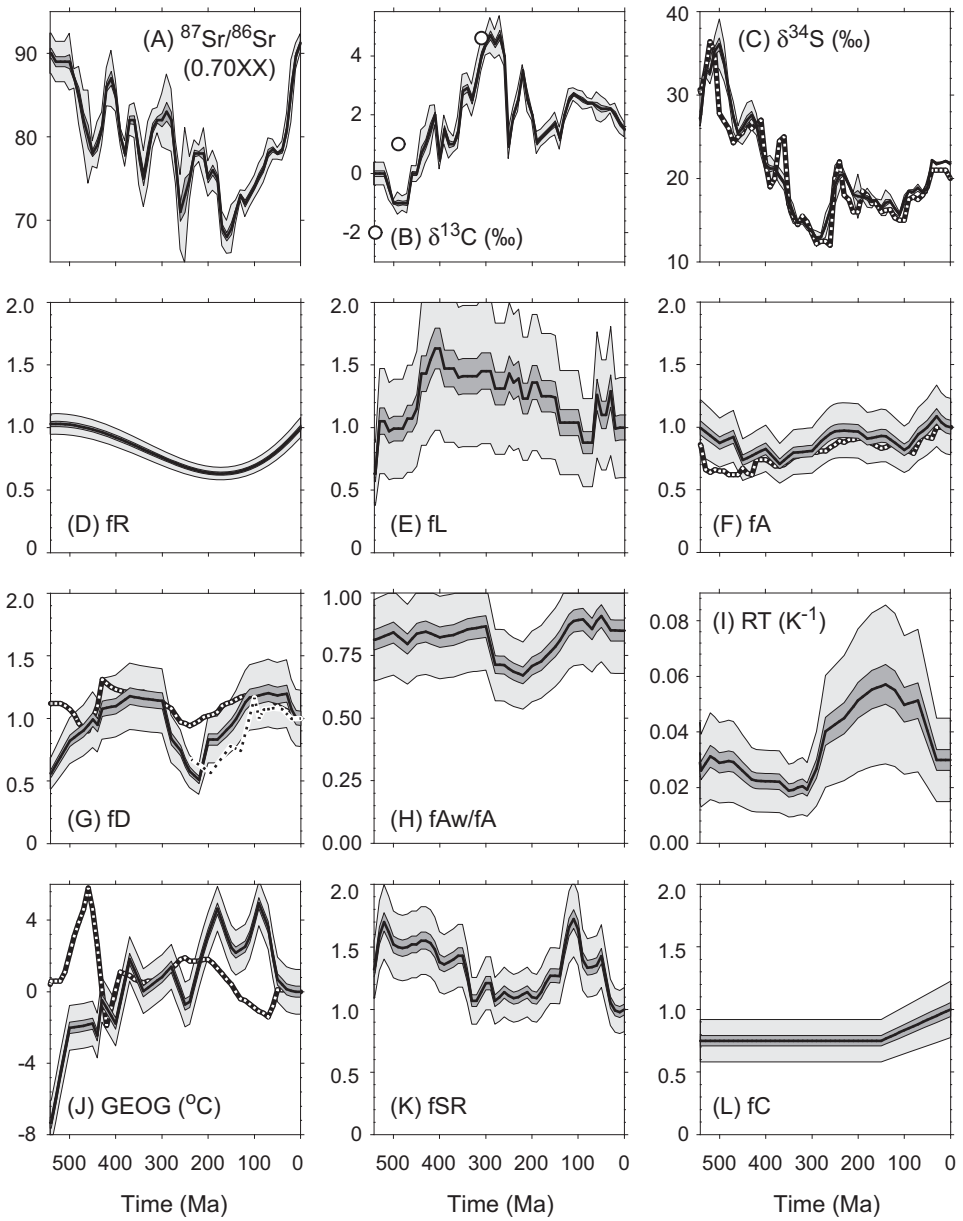

Fig. 1. Input arrays for the GEOCARBSULF model. See METHODS and Appendix 1 for descriptions of the arrays. (A) $^{87}Sr/^{86}Sr$ of shallow-marine carbonate, where the units are the third and fourth digits of the ratio (0.70XX). (B) $\delta^{13}C$ of shallow-marine carbonate. The three circles are values from the standard compilation that were adjusted to avoid excessive model failure (see METHODS for details). (C) $\delta^{34}S$ of marine sulfate. (D) *fR* = effect of relief on chemical weathering. (E) *fL* = land area covered by carbonates. (F) *fA* = land area. (G) *fD* = global river runoff. The black dashed line is from Gibbs and others (1999). (H) *fAw/fA* = fraction of land area undergoing chemical weathering (maximum value = 1). (I) *RT* = coefficient relating continental runoff to temperature change. (J) *GEOG* = land mean surface temperature. (K) *fSR* = seafloor creation rate. (L) *fC* = effect of carbonate content of subducting oceanic crust on CO_2 degassing rate. In panels C, F, G, and J, the white dashed lines are the older input arrays used by Berner (2004). In all panels, light shading is the $\pm 2\sigma$ associated with a sampling distribution that avoids >5% model failure when resampling only the array in question (all other input parameters held fixed); these are the variances reported in Appendix 1. Dark shading is the $\pm 2\sigma$ associated with a sampling distribution that avoids >5% model failure when resampling all input parameters simultaneously (75% reduction relative to the light shading).

the model fails at the 540-, 490-, and 310-Ma time-steps unless the variance of parameter deviations is almost zero (see circles in fig. 1B). As a compromise, we assign new values for each of these three data points by taking the mean of their adjacent two time-steps. For $\delta^{34}S$, we note high model failure in the standard GEOCARBSULF time series during the 570 to 560 Ma interval. Wu and others (2010) compile a $\delta^{34}S$ time series that largely mirrors the GEOCARBSULF standard (compare lines in fig. 1C) except with additional Cambrian values that eliminate the problem with model failure. We therefore adopt the Wu compilation for sulfate $\delta^{34}S$. This adoption causes negligible changes to estimates of Phanerozoic CO_2 and O_2.

Paleogeography time series (f_R, f_L, f_A, f_D, f_{Aw}/f_A, RT, and GEOG).—Continental relief affects silicate weathering because steeper terrains are more likely to expose fresh minerals to surface conditions (for summary, see Berner, 2004; see also Maher and Chamberlain, 2014). In GEOCARBSULF, f_R is defined as the effect of relief on chemical weathering at time (t) relative to the present-day. Early GEOCARB models use marine carbonate $^{87}Sr/^{86}Sr$ to estimate f_R while newer versions use rock-abundance compilations. Both approaches yield similar values for f_R (Berner, 2004); we use here f_R calculated from rock abundance (fig. 1D).

In GEOCARBSULF carbonate weathering is partly dependent on f_L, the fraction of total land area covered by carbonates at time (t) relative to the present-day. Because carbonates weather much faster than silicates, continental relief (f_R) is not thought to be an important controlling factor. GEOCARBSULF uses the Phanerozoic f_L compilation of Bluth and Kump (1991) (fig. 1E). Carbonate weathering has little direct effect on atmospheric CO_2 over multi-million-year timescales because carbonate formation consumes the same amount of CO_2 as is released for an equivalent mass of carbonate undergoing chemical weathering. However, the global rate of carbonate weathering affects marine alkalinity and, thus, carbonate precipitation rates (a sink for atmospheric CO_2 for carbon derived from silicate weathering reactions); it also affects, in the long-term, degassing from volcanism, metamorphism, and diagenesis.

In order to scale f_L to a weathering flux, total exposed land area is needed. This need is especially apparent given that most changes in total land area occur along continental margins, which often contain carbonate-rich sediments. Berner (2006a) makes a similar argument for the weathering of $CaSO_4$ sulfur, young organic matter, and young pyrite sulfur. Total land area may also affect silicate weathering rates, but this effect is considered minor because continental margins are typically low-relief areas containing highly weathered or recalcitrant silicate minerals (Berner, 2004). In GEOCARBSULF f_A is the land area at time (t) relative to the present-day. The standard data set for f_A comes from Otto-Bliesner (1995), who calculates f_A for 14 time-slices based on paleogeographic maps (white dashed line in fig. 1F). Goddéris and others (2012) provide updated f_A values for 22 time-slices. Here we adopt the Goddéris compilation, linearly interpolating between data points where necessary; the difference between the two f_A data sets is minor, except during the early Paleozoic (fig. 1F).

Global runoff provides an important constraint on the chemical weathering of silicates, carbonates, and $CaSO_4$ sulfur (Berner, 2006a; Maher and Chamberlain, 2014). f_D in GEOCARBSULF is defined as the global river runoff at time (t) relative to the present-day excluding the effects of changing CO_2 and solar luminosity. Otto-Bliesner (1995) provides the data set for f_D typically used in GEOCARBSULF (white dashed line in fig. 1G), but we adopt here values from Goddéris and others (2012). Because their runoff calculations incorporate changing CO_2 and solar luminosity, Y.D. ran the Goddéris simulations at fixed present-day levels of CO_2 and luminosity to match the GEOCARBSULF input format (fig. 1G). In these simulations, we allow continental ice sheet growth only during known times of long-lived, widespread glaciation (the late Paleozoic and late Cenozoic, 330-260 Ma and 34-0 Ma); otherwise,

the model generates large ice sheets for the entire Phanerozoic. This approach differs from Otto-Bliesner (1995), who universally excludes ice sheets. Goddéris and others (2012) also couple their GCM to a vegetation model for time-slices younger than the middle Devonian, while Otto-Bliesner (1995) excludes vegetation and prescribes a fixed snow-free albedo. Finally, the Goddéris model has a higher spatial resolution (7.5°×4.5° vs. 11.5°×11.5°) and includes a parameterization of topography (Otto-Bliesner assumes no topography).

f_D values are significantly lower in the Goddéris simulation during the late Paleozoic and early Mesozoic, probably due to the reasons just described. Importantly, these lower values are consistent with the independent study of Gibbs and others (1999) (black dashed line in fig. 1G). From the perspective of silicate weathering, lower f_D values result in higher CO_2 levels. To modulate the silicate-weathering flux, f_D must be multiplied by land area and scaled for dilution of HCO_3^- (exp_fD in Appendix 2; see Berner, 1994, 2004). Previously in GEOCARBSULF, f_A was used for the land-area term, but here we calculate from the simulations of Goddéris and others (2012) the land-area fraction that actually undergoes chemical weathering (f_{Aw}/f_A; fig. 1H), which we take as any grid cell with a non-zero runoff. In combination with f_A to form the time series (f_{Aw}/f_A) x f_A x f_D = $f_{Aw}f_D$, this expression more realistically depicts chemical weathering in the past and results in higher estimates of atmospheric CO_2.

The climatic effects on f_D are treated separately. The generic response of temperature change on f_D at each time-step, called *RT*, is taken from GCM simulations, where $f_D = 1+RT\times(T\text{-}T_0)$, T = global mean surface temperature at some past time (in K), and T_o = present-day global mean surface temperature (taken as 288 K). We adopt here the calculations of *RT* from Goddéris and others (2012) (fig. 1I), which produce only negligible differences in estimated CO_2 and O_2 relative to the *RT* values used previously in GEOCARBSULF.

Temperature is calculated partly from CO_2 assuming a prescribed climate sensitivity (ΔT_{2X}; described in next section) and from models of long-term solar evolution (Gough, 1981) (W_s in Appendix 2). Global-mean land-surface temperature is also affected by other factors, most importantly changes in paleogeography. In GEOCARBSULF, *GEOG* is the change in temperature relative to the present-day, assuming present-day CO_2 and solar luminosity. The standard compilation of *GEOG* comes from the GCM simulations of Otto-Bliesner (1995) (white dashed line in fig. 1J). Goddéris and others (2012) present alternate *GEOG* values that we recalculate for present-day CO_2 and luminosity and adopt for our simulations (fig. 1J). Similar to f_{Aw}/f_A, in calculating *GEOG* we only include grid cells with non-zero runoff (that is, non-zero chemical weathering). This marks a critical advance over previous implementations of GEOCARBSULF because we now exclude cold and dry environments (Berner and Kothavala, 2001; Berner, 2004). Our new *GEOG* formulation is warmer during the Mesozoic and cooler during the early Paleozoic (fig. 1J).

Degassing (f_{SR} and f_C).—Seafloor spreading rates exert strong control on volcanic and metamorphic degassing rates, a major source of CO_2 and sulfur on geologic timescales (Berner, 2004). GEOCARBSULF defines f_{SR} as the seafloor creation rate at time (t) relative to the present-day. Spreading rates are inferred from the volume of intact seafloor and, for times predating intact seafloor (>180 Ma), from global sea level (fig. 1K). Berner (2004) considers this variable one of the most poorly constrained (see also, for example, Rowley, 2002; Lee and others, 2013; van der Meer and others, 2014).

Prior to the evolution of calcareous plankton ~150 Ma, most marine carbonate deposition occurred in coastal environments overlying cratons, which were less likely to subduct. Over the last 150 m.y., more carbonate has been deposited in pelagic sediments overlying oceanic plates, which are more likely to subduct (Wilkinson and

Walker, 1989; Arvidson and others, 2014). In GEOCARBSULF, f_C is the effect of CO_2 degassing rate at time (t), relative to the present-day, caused by carbonate sediments on subducting oceanic crust. Following Wilkinson and Walker (1989), GEOCARBSULF assumes a value of 0.75 prior to 150 Ma, ramping linearly to 1 at the present-day (Berner, 2004) (fig. 1L).

Parameters Considered in Study: Constants

GEOCARBSULF contains 56 time-invariant parameters. We describe first the 15 constants that modify the carbon and sulfur fluxes (Appendix 2); we then briefly describe the 41 constants that define boundary conditions at 570 Ma and the present-day (Appendix 3).

Chemical weathering (ACT, ACT_{carb}, VNV, NV, and exp_NV).—The activation energy (ΔE; kJ mol^{-1}) for the dissolution of calcium and magnesium silicate rocks on land affects chemical weathering rates. In GEOCARBSULF, the input constant *ACT* is related to ΔE: $ACT = \Delta E/R \times T \times T_0$, where R = gas constant (0.008314 kJ mol^{-1} K^{-1}). This factor has been heavily studied in the field and laboratory (for a summary see Berner, 2004) and is one of the better-constrained constants in GEOCARBSULF. Following Berner (2004), we assume a best-fit value of 0.09 K^{-1} (ΔE = 55 kJ mol^{-1} for the present-day). There is little evidence in the present-day for *ACT* outside the bounds 0.03-0.13 K^{-1} (ΔE = 20-90 kJ mol^{-1}). ACT_{carb} is an analogous expression for carbonate weathering that includes the effects of temperature and CO_2 (0.087 K^{-1}) (Drake and Wigley, 1975).

The rate of chemical weathering in volcanic silicate rocks is typically higher than that in non-volcanic silicate rocks. In GEOCARBSULF, *VNV* (or W_v/W_{nv}) expresses this ratio. Field studies suggest a mean value of 5, and values <2 or >10 are considered unlikely (Berner, 2006b, 2008). To scale this effect to all silicate land surfaces experiencing weathering, some knowledge of the fraction of these surfaces that are volcanic is needed (X_{volc}). In GEOCARBSULF, this is accomplished by modeling the key inputs of Sr (seawater $^{87}Sr/^{86}Sr$) and taking advantage of the contrasting $^{87}Sr/^{86}Sr$ values between volcanic and non-volcanic silicate rocks. For this, the parameters *NV* and exp_*NV* are introduced to scale physical erosion and chemical weathering to the mean $^{87}Sr/^{86}Sr$ value of non-volcanic silicate rocks (Berner, 2006b, 2008).

Plant-assisted weathering (LIFE, GYM, FERT, and exp_fnBb).—The presence of large vascular plants accelerates chemical weathering rates (Berner, 1992; Moulton and others, 2000). Watershed studies suggest that the effect is several-fold. Berner (2004) defines *LIFE* as the rate of chemical weathering in a minimally vegetated world relative to an angiosperm-dominated world and, based on a literature compilation, assumes a best-fit value of 0.25 (4-fold increase in rate) and a likely range of 0.125 to 0.5 (8- to 2-fold increase in rate).

Related to *LIFE*, *GYM* is the rate of chemical weathering by gymnosperms relative to angiosperms. This term is poorly constrained (Berner and Kothavala, 2001; Andrews and others, 2008). We adopt here the formulation of Berner (2004) that gymnosperms chemically weather at a lower rate (*GYM* = 0.875). In GEOCARBSULF, the efficacy of chemical weathering associated with *GYM* increases linearly to its full value between 380 to 350 Ma, coincident with the evolution of non-angiosperm forests. The efficacy of angiosperms is phased in linearly between 130 to 80 Ma, reflecting the evolution of angiosperm-dominated forests in most areas of the world.

Because plant productivity is stimulated by CO_2, plant-mediated chemical weathering is also sensitive to CO_2 (Andrews and Schlesinger, 2001; Baars and others, 2008; Gislason and others, 2009). *FERT* reflects the fraction of plants globally that are fertilized by increasing CO_2 and is related to enhanced chemical weathering by the Michaelis-Menten expression $[2RCO_2/(1+RCO_2)]^{FERT}$, where RCO_2 = mass of CO_2 at some time in the past relative to pre-industrial levels (250 ppm). We adopt the

GEOCARBSULF standard of 0.4 (12% increase in weathering with a CO_2 doubling), which mirrors the experimental results of Andrews and Schlesinger (2001).

In the absence of vascular plants, chemical weathering still responds to CO_2 via acidification of the regolith following the expression $(RCO_2)^{exp_fnBb}$; a likely value for *exp_fnBb* is 0.5 (Berner, 1992, 1994, 2004), corresponding to a 41 percent increase in chemical weathering rate with a CO_2 doubling.

Climate sensitivity (ΔT_{2X} and GLAC).—Temperature affects chemical weathering rates, both directly via activation rates (ΔE discussed earlier) and indirectly through changes in global rainfall. In GEOCARBSULF, temperature is calculated in part from atmospheric CO_2 using a climate sensitivity transformation. Estimates over a century suggest a "short-term" climate sensitivity (ΔT_{2X}) of ~3 K for a CO_2 doubling above pre-industrial levels, although the probability distributions are right-skewed and it is difficult to exclude very high values (Rohling and others, 2012; IPCC, 2013). In recognition of this skewness, we resample this parameter assuming a lognormal distribution and a mean value of 3 K; consistent with geologic studies, we exclude value choices below 1.5 K (Royer and others, 2007, 2012; Park and Royer, 2011).

These calculations of ΔT_{2X} ignore slower, long-term processes such as continental ice sheet dynamics. For a long-term geochemical model like GEOCARBSULF with a time-step of 10 m.y., a climate sensitivity that includes feedbacks on all timescales (up to 10 m.y.) is more appropriate. Geologic evidence supports a long-term climate sensitivity (sometimes called "Earth system sensitivity") during times with large continental ice sheets of 6 K or higher (Hansen and others, 2008; Pagani and others, 2010; Park and Royer, 2011; Rohling and others, 2012). In GEOCARBSULF, the parameter *GLAC* scales ΔT_{2X} during the two most extensive and long-lived Phanerozoic glaciations: the late Paleozoic (330-260 Ma) and late Cenozoic (34-0 Ma). Following Park and Royer (2011), we assume a mean value of 2 and exclude parameter choices below 1.

Isotopic fractionation coefficients (J and n).—GEOCARBSULF uses the $\delta^{13}C$ of organic matter and $\delta^{34}S$ of pyrite sulfur to track the burial flux (marine + terrestrial) of organic matter and pyrite. Extensive Phanerozoic records are not presently available (Hayes and others, 1999; Beerling and others, 2002; Berner, 2009; Wu and others, 2010), but experiments (Berner and others, 2000; Beerling and others, 2002) and theory (Canfield and Teske, 1996) identify a sensitivity to atmospheric O_2 in the isotopic fractionation between reduced and oxidized forms of carbon and sulfur. GEOCARBSULF exploits this sensitivity to calculate the isotopic fractionations between organic and carbonate carbon ($\Delta^{13}C$) and between pyrite and $CaSO_4$ sulfur ($\Delta^{34}S$) using the following relationships (Berner and others, 2000):

$$\Delta^{13}C = \Delta^{13}C^{(0)} + J \times (O_2/O_2^{(0)} - 1) \quad (3)$$

$$\Delta^{34}S = \Delta^{34}S^{(0)} \times (O_2/O_2^{(0)})^n \quad (4)$$

where the superscript "(0)" refers to the present-day (see Appendix 3) and oxygen is expressed in units of mass. From equations (3) and (4) GEOCARBSULF computes organic carbon and pyrite isotopic values from the more complete times series of carbonate and sulfate isotopic values. Values of $J = 4$ and $n = 1.5$ fit experimental and theoretical constraints well, and produce calculated values of $\Delta^{13}C$ and $\Delta^{34}S$ for the Phanerozoic that broadly match existing records (Berner and others, 2000; Berner, 2001, 2009; Beerling and others, 2002). In our simulations, $n = 1.5$ results in high model failure rate during the early Paleozoic, even with a small 2σ. Consequently, our preferred mean value is 1 (Appendix 2); this change has very little effect on estimated O_2.

Other constants related to initial or present-day conditions.—There are 41 additional input parameters that describe a flux, rate, mass, or isotopic composition for the

present-day or initial (570 Ma) conditions in GEOCARBSULF (Appendix 3). Most of these parameters are recalculated at each time-step (variables superscripted with "(0)" and "(570)" in Appendix 3), but some are assumed fixed (variables without a numeric suffix in Appendix 3).

The Code and Resampling Strategy

D.L.R. wrote scripts in the R processing language to run GEOCARBSULF and the associated resampling routines (R Core Team, 2014). The GEOCARBSULF code comes mostly from a translation of the BASIC scripts written by R.A. Berner (accessed in October 2013), with some modifications following the FORTRAN scripts written by J.P. for Park and Royer (2011). The code and input files are archived at figshare (http://dx.doi.org/10.6084/m9.figshare.902207) and also linked from D.L.R.'s academic website (http://droyer.web.wesleyan.edu). The code is annotated sufficiently to allow use by the broader community, including those without a programming background. All presented simulations calculate CO_2 every 10 m.y. and assume steady-state between time steps (Berner, 2004). Because the study focuses on the Phanerozoic, we mostly ignore CO_2 and O_2 values from the first three time-steps (570-550 Ma).

We test the sensitivity of estimated CO_2 and O_2 to all 68 input parameters in GEOCARBSULF, both singly and in combination. We quantify sensitivity in the model with Monte Carlo simulations. For testing each parameter singly, we generate 10000 values that are constrained by its range; for time series, we generate 10000 values for each 10 m.y. time-step (Appendices 1-3; fig. 1). We assume a Gaussian distribution for all parameters except climate sensitivity (ΔT_{2X}), for which we assume a lognormal distribution (see earlier discussion). For most parameters, some values are highly unlikely or impossible (for example, negative values for most parameters; see Appendices 1-3); when such values are drawn randomly, they are assigned a value just inside (0.0001) the allowable range. In our model set up, these substitutions are extremely rare (compare means and 2σ with the lower and upper limits in Appendices 1-3). Once the resampled matrix is populated, the GEOCARBSULF model is run 10000 times using the resampled values; all other input parameters are held fixed at their mean values. The strategy for testing combinations of parameters is similar, except that multiple sets of 10000 values are drawn, one for each tested parameter. All presented error envelopes for CO_2 and O_2 correspond to the 2.5 and 97.5 percentiles (that is, the inner 95% of calculated values).

For most input parameters, assigning a quantitative uncertainty is difficult due to a general lack of knowledge. Climate sensitivity (ΔT_{2X}) is one of the better-constrained variables, owing to over a century of work. We adopt here a 2σ of ±2.5 K, which closely matches many independent assessments (95% of value choices fall between 1.5-7.3 K) (Rohling and others, 2012; IPCC, 2013). For the isotopic records ($^{87}Sr/^{86}Sr$, $\delta^{13}C$, $\delta^{34}S$), our arrays do not have reported uncertainties; we therefore compute and adopt the 10 m.y. time-step 2σ from Prokoph and others (2008). For the twelve isotopic constants (see Appendix 3), we use the mean time-step 2σ from Prokoph and others (2008) (0.0021, 2.1‰, and 4.7‰ for $^{87}Sr/^{86}Sr$, $\delta^{13}C$, and $\delta^{34}S$, respectively). For *GEOG*, we assume a 2σ of ±5 K, which matches its temporal variability (fig. 1J). For the remaining 51 input parameters, we conservatively assume that the 2σ ranges do not exceed ±50 percent of their means.

An important constraint for identifying probable input ranges is whether or not a set of value choices leads to model failure. GEOCARBSULF can fail at a particular time-step for the following four reasons. (1) One (or more) of the carbon or sulfur fluxes goes negative, reflecting an infeasible combination of input parameter choices. (2) Estimated O_2 is <5 percent or >50 percent of Earth's atmosphere, which are values beyond the constraints imposed by plant flammability studies and the geologic record of wildfire (≈10-40%) (Berner and others, 2003; Wildman and others, 2004;

Scott and Glasspool, 2006; Belcher and McElwain, 2008). (3) Estimated CO_2 is <150 ppm or >50000 ppm, which are values well outside the bounds imposed by independent records of CO_2 from proxies (Royer, 2014) and the physiological principles of plant starvation (Ward and others, 2005). We note CO_2 and O_2 likely fall well inside these bounds for most of the Phanerozoic, leading us to possibly overestimate the true uncertainty in estimated CO_2 and O_2. (4) Estimated CO_2 or O_2 for the pre-industrial present-day (t = 0 Ma in the model) deviate from their measured values (CO_2: outside the 200-300 ppm range; O_2: outside the 19-23% range). The most likely reason for the final kind of model failure is incorrect choices for the initial masses or isotopic values (Berner, 2006a). When GEOCARBSULF fails for this reason, we consider the entire time series for the particular resample a failure.

When we run GEOCARBSULF with the 2σ ranges just described, >99 percent of the evaluated time-steps fail by our criteria (we perform this simulation with one million resamples to ensure almost 10000 valid evaluations at each time-step). This means that some of prescribed parameter variances are probably too large. To establish more realistic variances we first analyze the small proportion of successful runs, but we find no appreciable differences in input parameter mean or variance relative to the initial prescriptions. Therefore our next strategy is to evaluate the model sensitivity of each input parameter singly, holding all other parameters fixed. If model failure exceeds 5 percent at any time-step, we reduce 2σ until model failure at all time-steps is <5 percent; for the time-dependent arrays, we reduce the variances in all time-steps proportionately. These are the 2σ reported in Appendices 2 and 3 and plotted as light gray envelopes in figure 1; the percent reduction in 2σ relative to initial values is also given in Appendices 1, 2, and 3. When we run GEOCARBSULF with simultaneous resampling of these revised input parameters, failure rate at all time-steps still exceeds 80 percent because we are now propagating 68 errors and exploring more model space (we perform this simulation with 100000 resamples to ensure >10000 valid evaluations at each time-step). This means that some of the parameter variances are still too large, but owing to the multi-dimensional nature of the model it is difficult to rigorously address the problem. We therefore calculate CO_2 and O_2 with these input ranges and assume that the calculated deviations in CO_2 and O_2 are too large (see the light gray envelopes in figs. 2, 3, and 4).

To explore the lower limits of error in the model, we proportionately reduce the variances in all parameters together until the failure rate at all time-steps is <5 percent. For our model-parameter choices, this requires a 75 percent reduction in 2σ (for time-dependent arrays, see the dark gray envelopes in fig. 1). Because the sensitivity in estimated CO_2 and O_2 to input parameter variation differs from parameter to parameter, we are probably reducing too far the variances of the less-sensitive parameters. The 95 percent confidence intervals for CO_2 and O_2 from this set of parameter variances correspond to the dark gray envelopes in figures 2, 3, and 4.

Within the framework of our model parameterization, deviations in estimated CO_2 and O_2 probably lie between the light gray and dark gray envelopes. We additionally note that our deviation bounds for *ACT*, *VNV*, and *LIFE* all fall within their observed present-day limits (see previous section). Nevertheless, our error envelopes may not fully reflect the true uncertainty in estimated CO_2 and O_2 for at least two reasons. First, GEOCARBSULF is a simplification of the long-term carbon and sulfur cycles; important processes may be missing. Second, we use the boundaries of model failure to largely shape the input parameter variances. While this approach has the paradoxical behavior of progressively reducing variances as more and more parameters are included, it is dependent on the parameter means being (mostly) correct. If enough means are poorly prescribed, the calculated variances will be wrong too. In

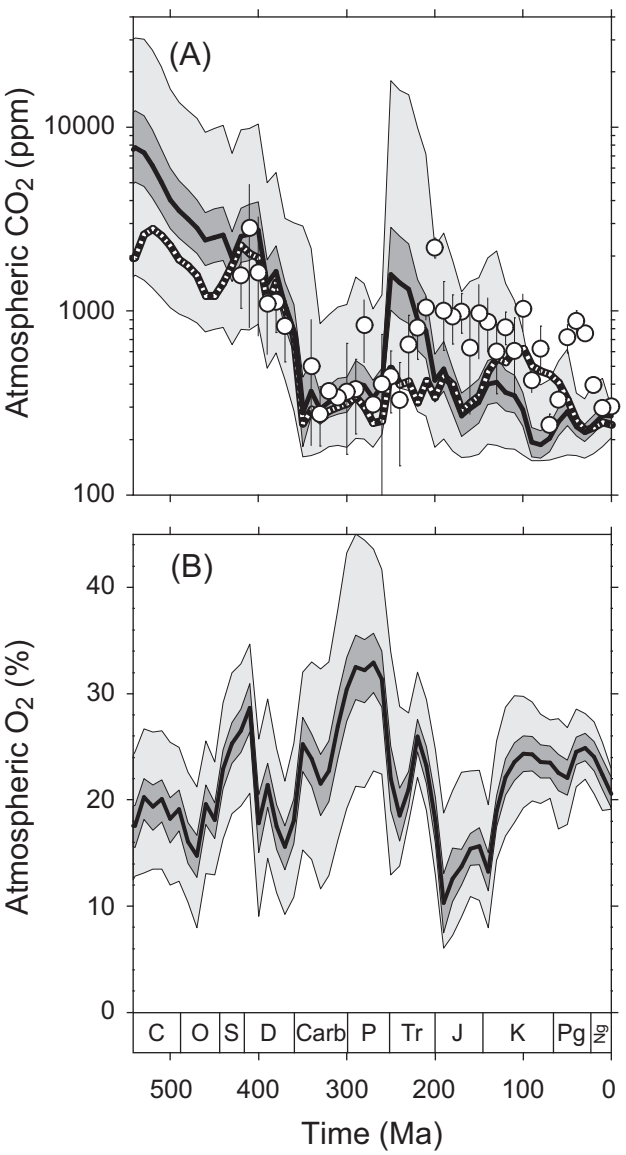

Fig. 2. Effect on calculations of atmospheric CO_2 and O_2 from GEOCARBSULF by co-variation of 68 input parameters. Black lines are the medians. Light gray envelopes encompass 2.5-97.5 percentile levels (that is, 95% of all calculations) for the input ranges presented in Appendices 1-3. Dark gray envelopes encompass 2.5-97.5 percentile levels after input ranges are further reduced by 75%. See METHODS for details. (A) Atmospheric CO_2. White dashed line uses the older formulations from Berner (2004) for land area (f_A), fraction of land area undergoing chemical weathering (f_{Aw}/f_A), global river runoff (f_D), and land mean surface temperature (*GEOG*). Circles are CO_2 calculated from CO_2 proxies, outputted in 10 m.y. time-steps; data set is updated from Royer (2014) ($n = 829$). Using the reported mean and lower bound and assuming a Gaussian distribution, error for each proxy estimate is simulated through 10000 random resamples. 10 m.y. time-steps are the medians of the 10000 rounds of resampling; errors are the 2.5 and 97.5 percentiles. (B) Atmospheric O_2.

short, while we consider our analysis the most robust yet of its kind, it should be viewed as a "work in progress".

RESULTS

All versions of GEOCARBSULF identify a "double-hump" pattern in CO_2, with higher values during the early Paleozoic and Mesozoic, and lower values during the late Paleozoic and Cenozoic. Our sensitivity analyses suggest that this first-order pattern is robust (envelopes in fig. 2A). For atmospheric O_2, the most striking pattern in GEOCARBSULF is a spike during the late Paleozoic (300-260 Ma). Here, our sensitivity analyses cannot reject the hypothesis of largely unchanging O_2, but this would require repeated shifts from one edge of our outer error envelope to another (light gray envelope in fig. 2B). We consider this scenario unlikely. The two best-resolved features of the O_2 record are a late Paleozoic peak (>30%) followed by a two-stage decline to the lowest values near the Triassic-Jurassic boundary (~10%).

The new formulations from Goddéris and others (2012) for land area (f_A), fraction of land area undergoing chemical weathering (f_{Aw}/f_A), runoff (f_D), and continental temperature (*GEOG*) affect estimated CO_2, most notably towards higher values during the early Paleozoic (542-430 Ma) and early Mesozoic (250-200 Ma) and lower values during the late Mesozoic to Cenozoic (130-50 Ma; compare black and white dashed lines in fig. 2A); the corresponding changes in O_2 are very small and are not shown in figure 2B.

For CO_2, our model simulations can be compared to independent records from proxies (white circles in fig. 2A are the 10 m.y. time-steps). We find excellent agreement during the Paleozoic (542-250 Ma), but strong differences during the late Mesozoic to early Cenozoic (~200-30 Ma): around 1000 ppm for the proxies versus 200 to 500 ppm for GEOCARBSULF.

An evaluation of the input parameters singly reveals the contribution of each to the overall deviations in figure 2 and to the observed differences in CO_2 between the traditional implementation of GEOCARBSULF versus with the new input arrays from Goddéris and others (2012). Figures 3 and 4 summarize the input parameters whose variances in our model set-up have the most influence on estimated CO_2 and O_2. Climate sensitivity (ΔT_{2X}) has the single biggest effect on CO_2, especially when estimated CO_2 is high (fig. 3A); here, the lower limit of the light gray error envelope corresponds to a ΔT_{2X} of 7.3 K per CO_2 doubling while the upper limit is tied to a ΔT_{2X} of 1.5 K per CO_2 doubling. Two factors related to plant-assisted chemical weathering, *LIFE* and *GYM*, have the next biggest impacts on estimated CO_2 (figs. 3B-3C). The lower limits of the light gray envelopes are associated with *LIFE* = 0.38, which implies a 2.6-fold increase in chemical weathering for angiosperm-dominated systems over minimally vegetated systems, and *GYM* = 1.29, which implies that gymnosperms induce 29 percent faster chemical weathering than angiosperms. The upper limits are associated with *LIFE* = 0.12 (8.3-fold weathering increase) and *GYM* = 0.46 (gymnosperms weathering at 46% the rate of angiosperms).

The exponent that scales the direct effect of CO_2 on chemical weathering in the absence of vascular plants has a moderate impact on estimated CO_2 during the early Paleozoic (*exp_fnBb*; fig. 3D). Variance in solar evolution has the next biggest impact, especially for the earlier parts of the record (W_s; fig. 3E). Next in line, seven parameters have a similar impact on CO_2: land area (f_A; fig. 3F), runoff (f_D; fig. 3G), continental temperature (*GEOG*; fig. 3H), fraction of land area undergoing chemical weathering (f_{Aw}/f_A; fig. 3I), relief (f_R), seafloor spreading rates (f_{SR}), and the effect of carbonate content of subducting oceanic crust on CO_2 degassing (f_C). Values for the first four parameters (f_A, f_D, *GEOG*, and f_{Aw}/f_A) come from Goddéris and others (2012). The updated land-temperature parameter *GEOG* has profound effects on CO_2: colder values during the early Paleozoic (542-430 Ma; fig. 1J) result in much higher estimates

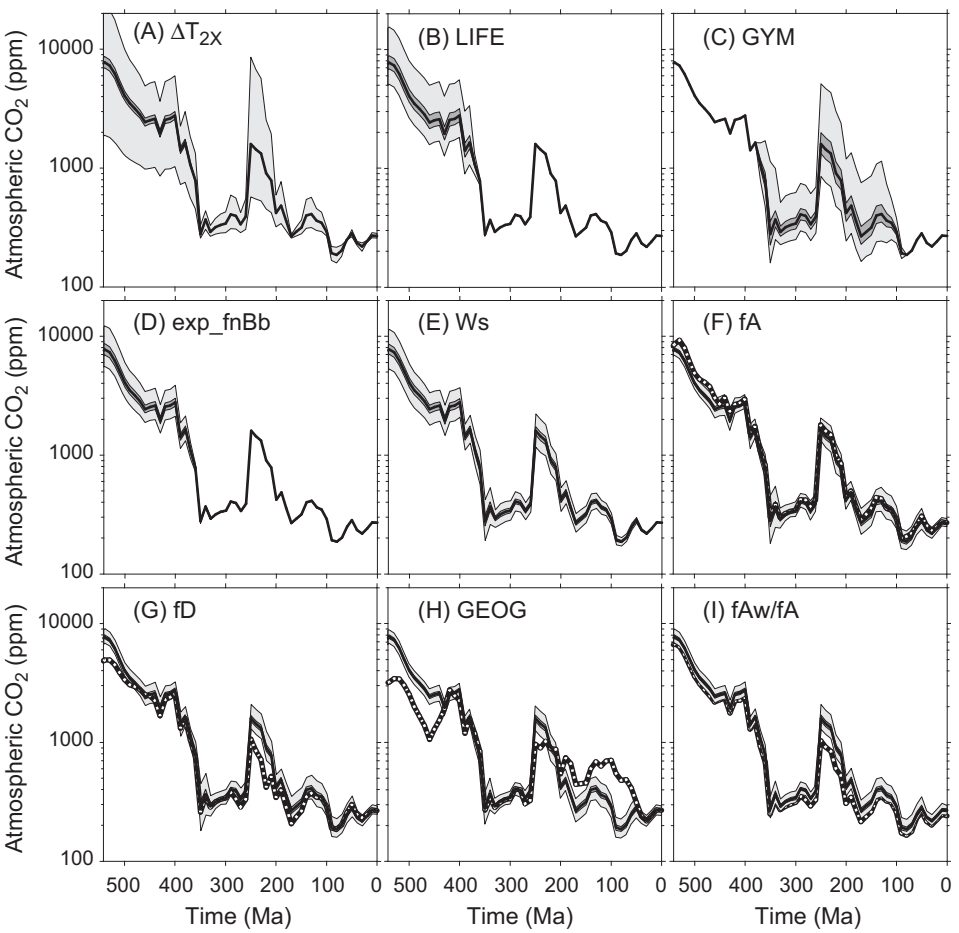

Fig. 3. Effect on calculations of atmospheric CO_2 by variation of a single input parameter. (A) ΔT_{2x} = climate sensitivity. (B) *LIFE* = ratio of chemical weathering in a minimally-vegetated to present-day (angiosperm dominated) world. (C) *GYM* = ratio of chemical weathering by gymnosperms to angiosperms. (D) *exp_fnBb* = direct effect of CO_2 on chemical weathering. (E) *Ws* = effect of solar evolution on temperature. (F) *fA* = land area. (G) *fD* = global river runoff. (H) *GEOG* = land mean surface temperature. (I) *fAw/fA* = fraction of land area undergoing chemical weathering. Black lines are the medians and are identical in all panels. In panels F-I, the white dashed lines use the older parameters from Berner (2004). Light gray envelopes encompass 2.5-97.5 percentile levels (that is, 95% of all calculations) for the input ranges presented in Appendices 1-3. Dark gray envelopes encompass 2.5-97.5 percentile levels after input ranges are further reduced by 75%.

of CO_2 (2000-8000 ppm versus 1000 to 3000 ppm with the traditional *GEOG* time series; compare black and white dashed lines in fig. 3H); similarly, warmer values during the Mesozoic to early Cenozoic (200-50 Ma) directly lead to considerably lower CO_2 estimates. For f_D, the new lower values during the late Paleozoic to early Mesozoic (fig. 1G) directly result in higher estimates of CO_2 (fig. 3G). f_{Aw}/f_A does not exist in older versions of GEOCARBSULF, but would be equivalent to a value of 1 (see also METHODS). The largest departure from 1 occurs during the late Paleozoic to early Mesozoic (fig. 1H); similar to f_D, this causes an increase in estimated CO_2 (fig. 3I). Finally, and in contrast to *GEOG*, f_D, and f_{Aw}/f_A, the new value choices for f_A have little effect on estimated CO_2 (fig. 3F); this is mostly because the two f_A data sets are very similar (fig. 1F).

Much of the uncertainties in CO_2 is explained by three input parameters (ΔT_{2X}, *LIFE*, and *GYM*; see figs. 3A-3C), while the contribution to deviations in O_2 is spread out more evenly (fig. 4). The parameters that most influence CO_2 do not overlap at all with the parameters that most influence O_2. The majority of these parameters for CO_2 involve the evaluation of chemical weathering, while most of those for O_2 involve isotopic records (which are used principally to track the burial of reduced carbon and sulfur) and the initial masses for reservoirs.

The major deviations in O_2 involve, in decreasing impact, (1) mass of young crustal carbonate carbon at 570 Ma ($C_y^{(570)}$) , (2) the $\delta^{13}C$ of carbonate carbon ($\delta^{13}C$), (3) the stable carbon isotope fractionation between carbonate and organic matter at present-day ($\Delta^{13}C^{(0)}$), (4) the mass of old $CaSO_4$ sulfur (S_{sa}), (5) the $\delta^{34}S$ of the mass of sulfur in oceans plus "interacting rocks" (sulfur in rocks undergoing weathering, burial, *et cetera*) (δ_{st}), and (6) the rate of mass dependence for young carbonate weathering (k_{wcy}) (figs. 4A-4F). Variation in the mass of old pyrite sulfur (S_{pa}), the mass of sulfur in oceans and "interacting rocks" (S_t), and land area (f_A) also exert some influence on estimated O_2 (figs. 4G-4I).

We note that our strategy of using model failure to establish input variances results in disproportionate variance reductions. For example, the following parameters had their variances reduced by >50 percent relative to their initial values: carbonate $\delta^{13}C$, sulfate $\delta^{34}S$, continental relief (f_R), land area (f_A), global river runoff (f_D), fraction of land area undergoing chemical weathering (f_{Aw}/f_A), land temperature (*GEOG*), seafloor creation rate (f_{SR}), carbonate content of subducting oceanic crust (f_C), present-day degassing of carbonates ($F_{mc}^{(0)}$), present-day silicate weathering flux ($F_{wsi}^{(0)}$), present-day fraction of silicate weathering from volcanic rocks ($X_{volc}^{(0)}$), mass of old crustal organic carbon (G_a), and mass and $\delta^{13}C$ of carbon in oceans and interacting rocks (C_t, δ_{ct}; Appendices 1 and 3). These parameters can also be considered sensitive in our execution of GEOCARBSULF, not in terms of creating large ranges in estimated CO_2 or O_2 but in terms of triggering model failure.

DISCUSSION

Our motivation was to test in GEOCARBSULF the probable space in estimated CO_2 and O_2. Because the probability distributions for most input parameters are poorly known, we took the approach of using the boundaries of model failure to shape the input distributions. Within our framework of model parameterization, we consider the likely distributions (at 95% confidence) of the input parameters and estimated CO_2 and O_2 to lie between the light and dark gray envelopes in figures 1-4. With these assumptions in mind, our most fundamental interpretation is that estimates of CO_2 and O_2 from GEOCARBSULF have discrete bounds that exclude some values. For example, it is highly unlikely that >1000 ppm CO_2 (integrated over the 10 m.y. time-step) existed during the late Paleozoic glaciation (fig. 2A). Furthermore, for CO_2 some of the temporal patterns are highly significant: most importantly, the "double-hump" pattern in Phanerozoic CO_2 identified in all versions of GEOCARBSULF and in other long-term carbon cycle models (for summary see Berner, 2004) is strongly supported by our analysis. Relative to previous implementations of GEOCARBSULF, we resolve a more pronounced CO_2 peak during the Triassic (compare solid and dashed lines in fig. 2A) owing to associated lower values for f_D, f_{Aw}/f_A, and *GEOG* (figs. 1G, 1H, and 1J); these changes, and associated drop in chemical weatherability, are largely a consequence of the dry continental interiors of Pangea (Goddéris and others, 2012, 2014). The temporal patterns in O_2 are statistically less distinct, but nonetheless our sensitivity analysis largely supports a Phanerozoic peak during the late Paleozoic followed by a low near the Triassic-Jurassic boundary (fig. 2B).

Estimates of O_2 are better constrained than estimates of CO_2: the outer error envelope averages ±30% of the median values for O_2 but +375%/−50% for CO_2

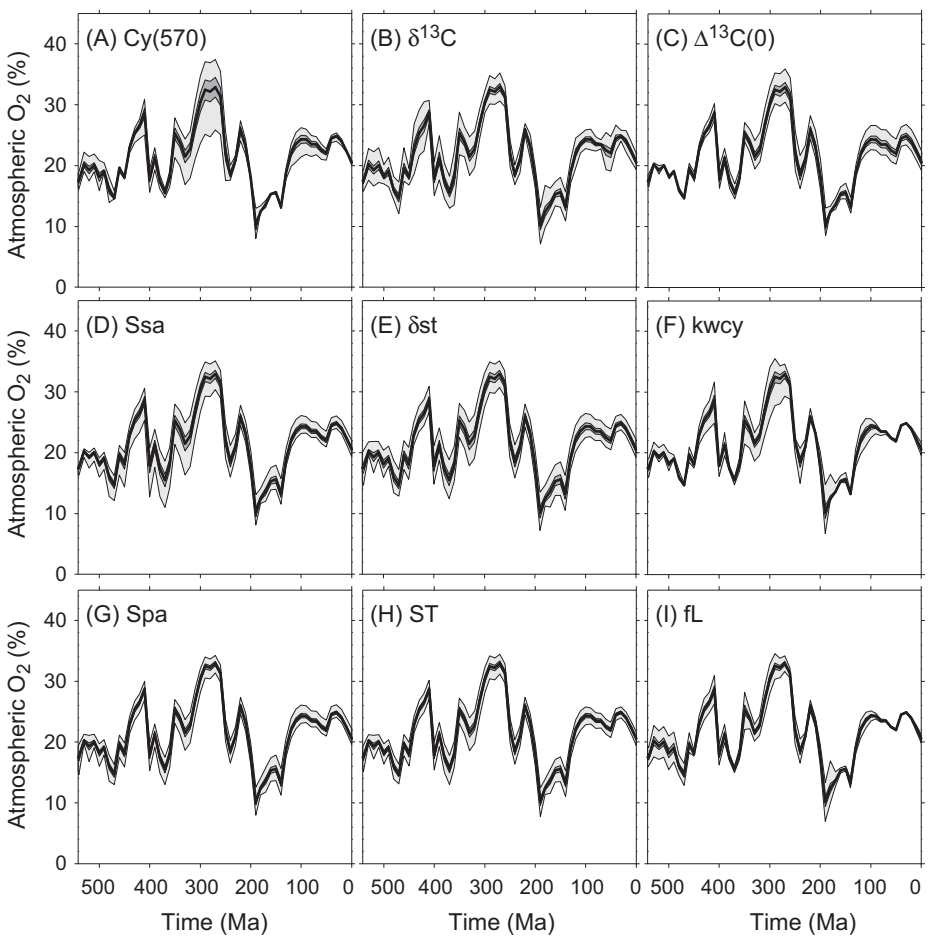

Fig. 4. Effect on calculations of atmospheric O_2 by variation of a single input parameter. (A) $C_y^{(570)}$ = Mass of young crustal carbonate carbon at 570 Ma. (B) $\delta^{13}C$ of shallow-marine carbonate. (C) $\Delta^{13}C^{(0)}$ = Fractionation between carbonate and organic matter at present-day. (D) S_{sa} = mass of old $CaSO_4$ sulfur. (E) $\delta_{st} = \delta^{34}S$ of sulfur in oceans and interacting rocks. (F) k_{wcy} = rate of mass dependence for young carbonate weathering. (G) S_{pa} = mass of old pyrite sulfur. (H) ST = mass of sulfur in oceans and interacting rocks. (I) fL = land area covered by carbonates. Black lines are the medians and are identical in all panels. Light gray envelopes encompass 2.5-97.5 percentile levels (that is, 95% of all calculations) for the input ranges presented in Appendices 1-3. Dark gray envelopes encompass 2.5-97.5 percentile levels after input ranges are further reduced by 75%. See METHODS for details.

(±10% vs. +40%/-25% for the inner error envelope). Errors in O_2 are nearly symmetrical, reflecting the linear combination of fluxes used to estimate O_2 (Berner, 2004). In contrast, the calculation of CO_2 includes several exponential scalings (for example, climate sensitivity and activation energy of Ca- and Mg-silicate dissolution; see Berner, 2004), resulting in asymmetric errors.

Several parameters influence the deviations in estimated O_2 almost equally (fig. 4). This means that reducing the variance in any one input parameter will not reduce dramatically the deviations in estimated O_2. In contrast, climate sensitivity (ΔT_{2X}) and the plant-assisted weathering factors *LIFE* and *GYM* contribute much of the deviations in GEOCARBSULF estimates of atmospheric CO_2. There is a long history of study for constraining ΔT_{2X} (Arrhenius, 1896; IPCC, 2013) and prospects for a significant

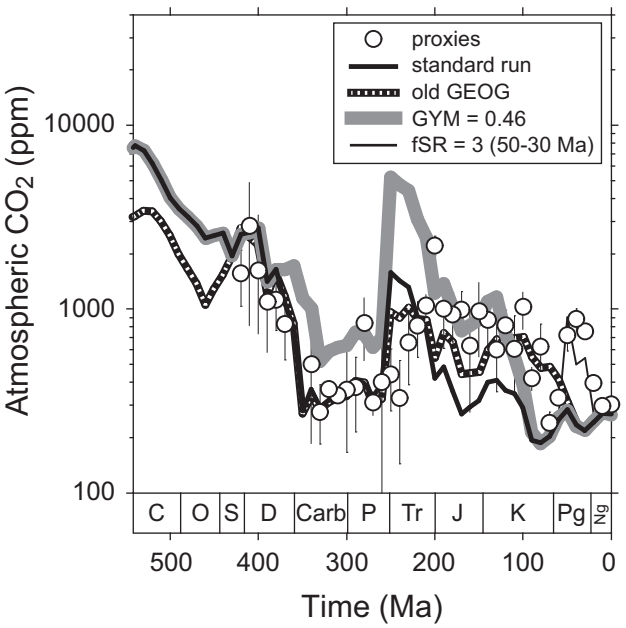

Fig. 5. Modifications to GEOCARBSULF to minimize misfit to CO_2 proxy records. White circles are the proxy records and thick black line is the standard GEOCARBSULF run; these are identically shown in figure 2A. Adjustments to the standard run are: use of the older input array from Berner (2004) for land mean surface temperature (*GEOG*; white dashed line; see dashed line in fig. 1J); ratio of chemical weathering by gymnosperms to angiosperms (*GYM*) = 0.46 (thick gray line); and seafloor creation rate (f_{SR}) = 3 for the 60-40 Ma time-steps (thin black line).

reduction in its uncertainty appear slim (Roe and Baker, 2007). Field studies provide some constraints for *LIFE* (Berner, 2004) and there is some promise for further reducing its uncertainty. *GYM* presently is poorly constrained (Berner, 2004; Andrews and others, 2008) and, if future studies can reduce its uncertainty, offers the most hope for reducing the uncertainty in Phanerozoic CO_2.

CO_2 proxies provide an independent cross-check on GEOCARBSULF estimates. Agreement is best for the older part of the record (Paleozoic to early Mesozoic; fig. 2A). For most of the last 200 m.y., the proxy record is considerably higher and more in keeping with the established view that globally warm climates dominated the period (Frakes and others, 1992; Vaughan, 2007; Price and others, 2013). Lee and others (2013) and van der Meer and others (2014) argue for a higher degassing rate that would largely eliminate this discrepancy up until 50 Ma. Alternatively, use of the traditional formulation for *GEOG* (dashed line in fig. 1J) goes some way in reconciling the mismatch in CO_2 during the Cretaceous (dashed line in fig. 5), although differences remain for the Triassic to Jurassic and early Cenozoic (see also discussion in Park and Royer, 2011). This highlights the need for further work to better elucidate the patterns of *GEOG* over the Phanerozoic. Alternatively, of the nine factors whose probable variance has the most influence on CO_2, changes in *GYM* offer the most promise for eliminating the discrepancy with proxies. If *GYM* is assigned a value of 0.46, which is the lower limit identified in our sensitivity analysis (Appendix 2), the associated GEOCARBSULF simulation during the Jurassic to Cretaceous matches the proxy record well (thick gray line fig. 5). However, CO_2 is seemingly too high during the late Paleozoic to Triassic (~350-200 Ma) and too low during the early Cenozoic (50-30 Ma), where the proxy record suggests values near 1000 ppm versus under 300

ppm in GEOCARBSULF. Changes in no single input parameter within its plausible range can realistically close the early Cenozoic gap (see fig. 3). For example, seafloor spreading rates—and associated degassing rates—would need to more than double (to values around three times the present-day rate) to force CO_2 estimates near 1000 ppm for this interval (thin black line in fig. 5). Such values are well outside current constraints (Cogné and Humler, 2006; Lee and others, 2013; Müller and others, 2013; van der Meer and others, 2014), including our sensitivity analyses (fig. 1K). The 50 to 30 Ma interval remains problematic for GEOCARBSULF.

Quantitative uncertainties for most input parameters in GEOCARBSULF are poorly known. Our strategy of calculating CO_2 and O_2 by resampling all 68 input parameters simultaneously—and rejecting parameter choices with a >5 percent likelihood for causing model failure—establishes tight uncertainties for many parameters. These quantitative uncertainties may prove useful for future studies, but as already discussed their veracity depends on two significant assumptions: that GEOCARBSULF is not missing any key processes, and that parameter means are correct. A critical next step for parameters whose variances were reduced the most is to assess the soundness of the trimmed variances. The carbonate $\delta^{13}C$ time series illustrates this issue well. We find that at many time-steps small deviations from the mean values lead to model failure. Following our strategy for establishing probable input distributions, this directly leads to a fairly tight resampling space (fig. 1B; see also METHODS). Prior to the age of the oldest intact seafloor (>180 Ma), data for this time series come mainly from epeiric sea sediments. Based on the analysis of rare Paleozoic open-ocean sediments, Brand and others (2009) argue that $\delta^{13}C$ values from epeiric seas may be lower than the open ocean by several per mil and therefore outside the range of our resampling space. But when we run GEOCARBSULF with these higher Paleozoic $\delta^{13}C$ values, even with no resampling, the model fails. From this, one interpretation is that the $\delta^{13}C$ record based on Brand and others (2009) is not representative of the open ocean. However, it is possible that the alternate $\delta^{13}C$ record is correct and either (1) GEOCARBSULF is missing some key processes or (2) values for other input parameters are incorrect. Presently, it is not clear which scenario is more plausible.

We highlight two limitations with the GEOCARBSULF model that may lead to points (1) and (2) just described. First, it is a zero-dimensional model. For example, GEOCARBSULF calculates a single global value of chemical weathering for each time-slice based on single, spatially averaged input parameters (for example, climate, lithology, vegetation). Goddéris, Donnadieu and colleagues have demonstrated the value of spatially resolving these input parameters (for example, Donnadieu and others, 2006; Goddéris and others, 2008a, 2008b, 2012, 2014; Nardin and others, 2011; Lefebvre and others, 2013). Results from this approach that are especially relevant to our study include higher CO_2 than GEOCARBSULF during the early-middle Jurassic (~200-180 Ma) (Goddéris and others, 2008a) and early Cenozoic (50-30 Ma) (Lefebvre and others, 2013). Spatially resolving appropriate input parameters for CO_2 estimates from GEOCARBSULF may therefore offer a robust alternative for reducing the misfits to CO_2 proxies and increasing the compatibility with paleotemperature records.

Second, many equations in GEOCARBSULF are based on parameterizations. That is, the equations are built on correlations and do not include an explicit physical description of the underlying processes (for example, the dependence of continental weathering as a function of climate, the dependence of global air temperature as a function of CO_2). While we explore the uncertainty of these relationships within the framework of our specific analysis, the model-dependence of the results could be reduced by substituting process-based calculations for some of the parametric laws of GEOCARBSULF. The inclusion of spatially-resolved temperature and runoff from

GCM modeling as already described would be a first step towards a more process-based description inside the GEOCARBSULF model, since GCMs explicitly solve for the energy and water budgets of the Earth surface.

CONCLUSION

Long-term carbon and sulfur cycle models have been used for decades to quantitatively reconstruct Phanerozoic patterns of atmospheric CO_2 and O_2 (for a review, see Royer, 2014). We performed a full error analysis for the GEOCARBSULF model, including new formulations for land area (f_A), fraction of land area undergoing chemical weathering (f_{Aw}/f_A), runoff (f_D), and continental temperature (*GEOG*). Our analysis strongly supports the presence of a "double-hump" pattern in atmospheric CO_2, with higher values during the early Paleozoic and Mesozoic and significantly lower values during the late Paleozoic and Cenozoic. Our analysis also provides support for a peak in atmospheric O_2 during the late Paleozoic followed by a drop to a Phanerozoic low near the Triassic-Jurassic boundary. Climate sensitivity (ΔT_{2X}) and two input parameters related to plant-assisted chemical weathering (*LIFE* and *GYM*) contribute most of the variance in estimated CO_2. Of the three, *GYM* shows the most promise for future improvements in precision.

GEOCARBSULF simulations of CO_2 compare favorably to independent records from proxies during the Paleozoic to early Mesozoic, but are considerably lower during the generally warm late Mesozoic to early Cenozoic (~200-30 Ma). Use of the traditional data set for *GEOG* and a formulation for *GYM* near its current lower bound of plausibility both go some way in eliminating the model-proxy mismatch, highlighting the need for better understanding these two factors. The mismatch during the early Cenozoic, however, cannot be resolved with changes to the input parameters within their plausible ranges. This implies that, for this interval, one or more parameters is in serious error or the model is missing some important processes.

ACKNOWLEDGMENTS

We thank R.A. Berner for sharing his GEOCARBSULF scripts and for helpful guidance. We also thank P.G. Resor for access to his computing cluster, S. Ewall for useful discussions, and P. Chamberlain, L. Kump, A. Ridgwell, and an anonymous reviewer for constructive reviews. Funding for this study has been partly provided by the French National Agency for Research (projects ANR-12-BS06-001 Anox-Sea and ANR-10-BLAN-0607 Terres).

Appendix

Table A1

Description of input arrays (time series)[a]

Array	Description [units]	Reduction in 2σ[b]	Lower bound[c]	Source[d]
Sr	$^{87}Sr/^{86}Sr$ of shallow-marine carbonate [$(^{87}Sr/^{86}Sr - 0.7)\times10^4$]	0		1-2
$\delta^{13}C$	$\delta^{13}C$ of shallow-marine carbonate [‰]	82		2-3
$\delta^{34}S$	$\delta^{34}S$ of marine sulfate [‰]	80		4
f_R	Effect of relief on chemical weathering at time (t) relative to the present-day	84	0	2
f_L	Land area covered by carbonates at time (t) relative to the present-day	20	0	2, 5
f_A	Land area at time (t) relative to the present-day	55	0	2, 6-7
f_D	Change in global river runoff at time (t) relative to the present-day in the absence of changing CO_2 and luminosity	55	0	2, 6-7
f_{Aw}/f_A	Fraction of land area undergoing chemical weathering	60	0	7
RT	Coefficient relating continental runoff to temperature change [1/K]	0	0	7
GEOG	Change in land mean surface temperature for areas experiencing chemical weathering at time (t) relative to the present-day in the absence of changing CO_2 and luminosity [K]	75		2, 6-7
f_{SR}	Seafloor creation rate at time (t) relative to the present-day	65	0	2
f_C	Effect of carbonate content of subducting oceanic crust on CO_2 degassing rate at time (t) relative to the present-day	55	0	2

[a] See figure 1 for plots of time series and their associated variances.

[b] Percent reduction in the initially prescribed variances required to avoid >5% model failure when resampling the parameter singly. These adjusted variances are plotted as the light gray envelopes in figure 1 and are used to calculate the light gray envelopes in figures 2-4. To calculate the dark gray envelopes in figures 1-4, variances are reduced further by 75%. See METHODS for details.

[c] Blank cells correspond to unbounded limits. f_{Aw}/f_A additionally has an upper bound of 1.

[d] These sources describe the time series. 1: Berner (1994); 2: Berner (2004); 3: Berner (2006a); 4: Wu and others (2010); 5: Bluth and Kump (1991); 6: Otto-Bliesner (1995); 7: Goddéris and others (2012).

TABLE A2

Description and resampling strategy of input constants

Variable	Description [units]	Mean	2σ[a]	Reduction in 2σ[b]	Lower bound[c]	Source[d]
ACT	Coefficient for activation energy of Ca- and Mg-silicate dissolution [1/K]	0.09	0.045	0	0	1
ACT_{carb}	Coefficient for activation energy of carbonate dissolution [1/K]	0.087	0.044	0	0	1
VNV	Rate ratio of chemical weathering in volcanic to non-volcanic silicate rocks	5	2.5	0	0	2-3
NV	Coefficient relating physical erosion to the mean $^{87}Sr/^{86}Sr$ of non-volcanic silicate rocks	0.0075	0.0038	0	0	3
exp_NV	Exponent related to *NV*	0.67	0.34	0	0	3
LIFE	Rate ratio of chemical weathering in a minimally vegetated to present-day (angiosperm dominated) world	0.25	0.13	0	0	1
GYM	Rate ratio of chemical weathering by gymnosperms to angiosperms	0.875	0.416	5	0	4-5
FERT	Exponent reflecting the fraction of plants globally that are fertilized by increasing CO_2 and that accelerate mineral weathering	0.4	0.2	0	0	4
exp_fnBb	Exponent that scales the direct effect of CO_2 on chemical weathering in the absence of vascular plants	0.5	0.13	50	0	1, 9
ΔT_{2X}	Climate sensitivity[e] [K per CO_2 doubling]	3	2.5	0	1.5	6-7
GLAC	Factor by which ΔT_{2X} changes during times with large continental ice sheets	2	1	0	1	6-7
J	Coefficient used to calculate $\delta^{13}C$ [‰]	4	2	0	0	8
n	Exponent used to calculate $\delta^{34}S$	1	0.5	0	0	8
W_s	Effect on temperature due to solar evolution [K per 570 m.y.]	7.4	3.7	0		1
exp_f_D	Exponent that scales the dilution of dissolved HCO_3^- with runoff (f_D)	0.65	0.33	0	0	1, 9

[a] These are used to calculate the light gray envelopes in figures 2-4. To calculate the dark gray envelopes in figures 2-4, variances are reduced further by 75%. See methods FOR DETAILS.

[b] Percent reduction in the initially prescribed variances required to avoid >5% model failure when resampling the parameter singly; the 2σ reported here already include this reduction. See METHODS for details.

[c] Blank cells correspond to unbounded limits. *FERT* additionally has an upper bound of 1.

[d] These sources describe the parameters and provide support for the value choices. 1: Berner (2004); 2: Berner (2006b); 3: Berner (2008); 4: Berner and Kothavala (2001); 5: Andrews and others (2008); 6: Park and Royer (2011); 7: Rohling and others (2012); 8: Berner (2006a); 9: Berner (1994).

[e] Resampled following a lognormal distribution.

TABLE A3

Description and resampling strategy of input constants that are a flux, rate, mass, or isotopic composition

Variable	Description[a]	Mean	2σ[b]	Reduction in 2σ[c]	Lower bound[d]	Source[e]
$F_{wpa}^{(0)}$	Sulfate flux from oxidative weathering of old pyrite at present-day	0.25	0.13	0	0	
$F_{wsa}^{(0)}$	Sulfate flux from weathering of $CaSO_4$ sulfur at present-day	0.5	0.25	0	0	
$F_{wga}^{(0)}$	Carbon flux from weathering of old sedimentary organic matter at present-day	0.5	0.25	0	0	
$F_{wca}^{(0)}$	Carbon flux from weathering of old carbonates at present-day	2	1	0	0	
$F_{mg}^{(0)}$	Carbon degassing flux of organic matter at present-day	1.25	0.63	0	0	1
$F_{mc}^{(0)}$	Carbon degassing flux of carbonates at present-day	6.67	1.50	55	0	1
$F_{mp}^{(0)}$	Sulfur degassing flux of pyrite at present-day	0.25	0.13	0	0	
$F_{ms}^{(0)}$	Sulfur degassing flux of $CaSO_4$ sulfur at present-day	0.5	0.25	0	0	
$F_{wsi}^{(0)}$	Weathering flux for all Ca and Mg silicates at present-day	6.67	0.83	75	0	2
$X_{volc}^{(0)}$	Fraction of total Ca and Mg silicate weathering derived from volcanic rocks at present-day	0.35	0.08	55	0	3-4
$\Delta^{13}C^{(0)}$	Fractionation between carbonate and organic matter at present-day	27	1.9	10	0	8
$\Delta^{34}S^{(0)}$	Fractionation between $CaSO_4$ sulfur and pyrite sulfur at present-day	35	4.7	0	0	8
$oxy^{(570)}$	Mass of atmospheric O_2 at 570 Ma	25	12.5	0	7.5	5
$G_y^{(570)}$	Mass of young crustal organic carbon at 570 Ma	250	63	50	0	5
$C_y^{(570)}$	Mass of young crustal carbonate carbon at 570 Ma	1000	475	5	0	5
$C_a^{(570)}$	Mass of old crustal carbonate carbon at 570 Ma	4000	1300	35	0	5
$S_{sy}^{(570)}$	Mass of young $CaSO_4$ sulfur at 570 Ma	150	56	25	0	5
$S_{py}^{(570)}$	Mass of young pyrite sulfur at 570 Ma	20	10	0	0	5
$\delta_{sy}^{(570)}$	$\delta^{34}S$ of young $CaSO_4$ sulfur at 570 Ma	35	4.7	0		5
$\delta_{cy}^{(570)}$	$\delta^{13}C$ of young carbonate carbon at 570 Ma	3	2.1	0		5
$\delta_{py}^{(570)}$	$\delta^{34}S$ of young pyrite sulfur at 570 Ma	-10	4.7	0		5
$\delta_{pa}^{(570)}$	$\delta^{34}S$ of old pyrite sulfur at 570 Ma	-10	4.7	0		5
$\delta_{gy}^{(570)}$	$\delta^{13}C$ of young organic matter at 570 Ma	-23.5	2.1	0		5
$\delta_{ga}^{(570)}$	$\delta^{13}C$ of old organic matter at 570 Ma	-23.5	2.1	0		5
$R_{cy}^{(570)}$	$^{87}Sr/^{86}Sr$ of young carbonates undergoing weathering at 570 Ma	0.7095	0.002	0		
$R_{ca}^{(570)}$	$^{87}Sr/^{86}Sr$ of old carbonates undergoing weathering at 570 Ma	0.709	0.002	0		
$R_g^{(570)}$	$^{87}Sr/^{86}Sr$ of non-volcanic silicates at 570 Ma	0.722	0.002	0		3
$R_v^{(570)}$	$^{87}Sr/^{86}Sr$ of sub-aerial and submarine volcanic rocks at 570 Ma	0.704	0.001	35		3
F_{ob}	Flux of Ca and Mg between basalt and seawater	4	2	0	0	3

TABLE A3
(continued)

Variable	Description[a]	Mean	2σ[b]	Reduction in 2σ[c]	Lower bound[d]	Source[e]
C_{oc}	Mass of carbon in ocean	2	1	0	0	
G_a	Mass of old crustal organic carbon	1000	75	85	0	5
S_{sa}	Mass of old $CaSO_4$ sulfur	150	75	0	0	5
S_{pa}	Mass of old pyrite sulfur	280	140	0	0	5
S_t	Mass of sulfur in oceans + "interacting rocks" (sulfur in rocks undergoing weathering, burial, etc.)	600	300	0	0	
δ_{st}	$\delta^{34}S$ of S_T	4	3.1	35		
C_t	Mass of carbon in oceans + "interacting rocks"	6252	469	85	0	1
δ_{ct}	$\delta^{13}C$ of C_T	-3.5	0.3	88		
k_{wpy}	Rate of mass dependence for young pyrite sulfur	0.01	0.005	0	0	5
k_{wsy}	Rate of mass dependence for young $CaSO_4$ sulfur	0.01	0.005	0	0	5
k_{wgy}	Rate of mass dependence for young organic matter weathering	0.018	0.009	0	0	5
k_{wcy}	Rate of mass dependence for young carbonate weathering	0.018	0.009	0	0	5

[a] Units are 10^{18} mol for masses, 10^{18} mol/m.y. for fluxes, m.y.$^{-1}$ for rates, and ‰ for stable isotopic compositions.
[b] These are used to calculate the light gray envelopes in figures 2-4. To calculate the dark gray envelopes in figures 2-4, variances are reduced further by 75%. See METHODS for details.
[c] Percent reduction in the initially prescribed variances required to avoid >5% model failure when resampling the parameter singly; the 2σ reported here already include this reduction. See METHODS for details.
[d] Blank cells correspond to unbounded limits. $X_{volc}^{(0)}$ additionally has an upper bound of 1. The lower bound for $oxy^{(570)}$ corresponds to 5%; it additionally has an upper bound of 143 10^{18} mol (equivalent to 50%).
[e] These sources describe the parameters and provide support for the value choices. 1: Berner (2004); 2: Berner (1991); 3: Berner (2008); 4: Berner (2006b); 5: Berner (2006a). Blank cells correspond to parameters whose values are reported here for the first time.

References

Andrews, J. A., and Schlesinger, W. H., 2001, Soil CO_2 dynamics, acidification, and chemical wethering in a temperate forest with experimental CO_2 enrichment: Global Biogeochemical Cycles, v. 15, n. 1, p. 149–162, http://dx.doi.org/10.1029/2000GB001278

Andrews, M. Y., Ague, J. J., and Berner, R. A., 2008, Weathering of soil minerals by angiosperm and gymnosperm trees: Mineralogical Magazine, v. 72, n. 1, p. 11–14, http://dx.doi.org/10.1180/minmag.2008.072.1.11

Arrhenius, S., 1896, On the influence of carbonic acid in the air upon the temperature on the ground: Philosophical Magazine and Journal of Science, v. 41, n. 251, p. 237–275, http://dx.doi.org/10.1080/14786449608620846

Arvidson, R. S., Mackenzie, F. T., and Berner, R. A., 2014, The sensitivity of the Phanerozoic inorganic carbon system to the onset of pelagic sedimentation: Aquatic Geochemistry, v. 20, n. 2–3, p. 343–362, http://dx.doi.org/10.1007/s10498-013-9224-5

Baars, C., Jones, T. H., and Edwards, D., 2008, Microcosm studies of the role of land plants in elevating soil carbon dioxide and chemical weathering: Global Biogeochemical Cycles, v. 22, n. 3, GB3019, http://dx.doi.org/10.1029/2008GB003228

Beerling, D. J., Lake, J. A., Berner, R. A., Hickey, L. J., Taylor, D. W., and Royer, D. L., 2002, Carbon isotope evidence implying high O_2/CO_2 ratios in the Permo-Carboniferous atmosphere: Geochimica et Cosmochimica Acta, v. 66, n. 21, p. 3757–3767, http://dx.doi.org/10.1016/S0016-7037(02)00901-8

Belcher, C. M., and McElwain, J. C., 2008, Limits for combustion in low O_2 redefine paleoatmospheric predictions for the Mesozoic: Science, v. 321, n. 5893, p. 1197–1200, http://dx.doi.org/10.1126/science.1160978

Berner, R. A., 1990, Atmospheric carbon dioxide levels over Phanerozoic time: Science, v. 249, n. 4975, p. 1382–1386, http://dx.doi.org/10.1126/science.249.4975.1382

——— 1991, A model for atmospheric CO_2 over Phanerozoic time: American Journal of Science, v. 291, n. 4, p. 339–376, http://dx.doi.org/10.2475/ajs.291.4.339

——— 1992, Weathering, plants, and the long-term carbon cycle: Geochimica et Cosmochimica Acta, v. 56, n. 8, p. 3225–3231, http://dx.doi.org/10.1016/0016-7037(92)90300-8

——— 1994, GEOCARB II: A revised model of atmospheric CO_2 over Phanerozoic time: American Journal of Science, v. 294, n. 1, p. 56–91, http://dx.doi.org/10.2475/ajs.294.1.56

——— 1997, The rise of plants and their effect on weathering and atmospheric CO_2: Science, v. 276, p. 544–546, http://dx.doi.org/10.1126/science.276.5312.544

——— 2001, Modeling atmospheric O_2 over Phanerozoic time: Geochimica et Cosmochimica Acta, v. 65, n. 5, p. 685–694, http://dx.doi.org/10.1016/S0016-7037(00)00572-X

——— 2004, The Phanerozoic Carbon Cycle: CO_2 and O_2: New York, Oxford University Press, 150 p.

——— 2006a, GEOCARBSULF: A combined model for Phanerozoic atmospheric O_2 and CO_2: Geochimica et Cosmochimica Acta, v. 70, n. 23, p. 5653–5664, http://dx.doi.org/10.1016/j.gca.2005.11.032

——— 2006b, Inclusion of the weathering of volcanic rocks in the GEOCARBSULF model: American Journal of Science, v. 306, n. 5, p. 295–302, http://dx.doi.org/10.2475/05.2006.01

——— 2008, Addendum to "Inclusion of the weathering of volcanic rocks in the GEOCARBSULF model" (R. A. Berner, 2006, v. 306, p. 295-302): American Journal of Science, v. 308, n. 1, p. 100–103, http://dx.doi.org/10.2475/01.2008.04

——— 2009, Phanerozoic atmospheric oxygen: New results using the GEOCARBSULF model: American Journal of Science, v. 309, n. 7, p. 603–606, http://dx.doi.org/10.2475/07.2009.03

Berner, R. A., and Kothavala, Z., 2001, GEOCARB III: A revised model of atmospheric CO_2 over Phanerozoic time: American Journal of Science, v. 301, n. 2, p. 182–204, http://dx.doi.org/10.2475/ajs.301.2.182

Berner, R. A., and Maasch, K. A., 1996, Chemical weathering and controls on atmospheric O_2 and CO_2: Fundamental principles were enunciated by J.J. Ebelmen in 1845: Geochimica et Cosmochimica Acta, v. 60, n. 9, p. 1633–1637, http://dx.doi.org/10.1016/0016-7037(96)00104-4

Berner, R. A., Lasaga, A. C., and Garrels, R. M., 1983, The carbonate-silicate geochemical cycle and its effect on atmospheric carbon dioxide over the past 100 million years: American Journal of Science, v. 283, n. 7, p. 641–683, http://dx.doi.org/10.2475/ajs.283.7.641

Berner, R. A., Petsch, S. T., Lake, J. A., Beerling, D. J., Popp, B. N., Lane, R. S., Laws, E. A., Westley, M. B., Cassar, N., Woodward, F. I., and Quick, W. P., 2000, Isotope fractionation and atmospheric oxygen: Implications for Phanerozoic O_2 evolution: Science, v. 287, n. 5458, p. 1630–1633, http://dx.doi.org/10.1126/science.287.5458.1630

Berner, R. A., Beerling, D. J., Dudley, R., Robinson, J. M., and Wildman, R. A., Jr. 2003, Phanerozoic atmospheric oxygen: Annual Review of Earth and Planetary Sciences, v. 31, p. 105–134, http://dx.doi.org/10.1146/annurev.earth.31.100901.141329

Bluth, G. J. S., and Kump, L. R., 1991, Phanerozoic paleogeology: American Journal of Science, v. 291, n. 3, p. 284–308, http://dx.doi.org/10.2475/ajs.291.3.284

Brand, U., Tazawa, J.-I., Sano, H., Azmy, K., and Lee, X., 2009, Is mid-late Paleozoic ocean-water chemistry coupled with epeiric seawater isotope records?: Geology, v. 37, n. 9, p. 823–826, http://dx.doi.org/10.1130/G30038A.1

Canfield, D. E., and Teske, A., 1996, Late Proterozoic rise in atmospheric oxygen concentration inferred from phylogenetic and sulphur-isotope studies: Science, v. 382, p. 127–132, http://dx.doi.org/10.1038/382127a0

Cogné, J.-P., and Humler, E., 2006, Trends and rhythmns in global seafloor generation rate: Geochemistry, Geophysics, Geosystems, v. 7, n. 3, Q03011, http://dx.doi.org/10.1029/2005GC001148

Donnadieu, Y., Goddéris, Y., Pierrehumbert, R. T., Dromart, G., Fluteau, F., and Jacob, R., 2006, A

GEOCLIM simulation of climatic and biogeochemical consequences of Pangea breakup: Geochemistry, Geophysics, Geosystems, v. 7, n. 11, Q11019, http://dx.doi.org/10.1029/2006GC001278
Drake, J. J., and Wigley, T. M. L., 1975, The effect of climate on the chemistry of carbonate groundwaters: Water Resources Research, v. 11, n. 6, p. 958–962, http://dx.doi.org/10.1029/WR011i006p00958
Ebelmen, J. J., 1845, Sur les produits de la décomposition des especes minérales de la famille des silicates: Annales des Mines, 4e série, v. 7, p. 3–66.
Frakes, L. A., Francis, J. E., and Syktus, J. I., 1992, Climate Modes of the Phanerozoic: Cambridge, Cambridge University Press, 274 p.
Gibbs, M. T., Bluth, G. J. S., Fawcett, P. J., and Kump, L. R., 1999, Global chemical erosion over the last 250 My: variations due to changes in paleogeography, paleoclimate, and paleogeology: American Journal of Science, v. 299, n. 7–9, p. 611–651, http://dx.doi.org/10.2475/ajs.299.7-9.611
Gislason, S. R., Oelkers, E. H., Eiriksdottir, E. S., Kardjilov, M. I., Gisladottir, G., Sigfusson, B., Snorrason, A., Elefsen, S., Hardardottir, J., Torssander, P., and Oskarsson, N., 2009, Direct evidence of the feedback between climate and weathering: Earth and Planetary Science Letters, v. 277, n. 1–2, p. 213–222, http://dx.doi.org/10.1016/j.epsl.2008.10.018
Goddéris, Y., Donnadieu, Y., Tombozafy, M., and Dessert, C., 2008a, Shield effect on continental weathering: Implication for climatic evolution of the Earth at the geological timescale: Geoderma, v. 145, n. 3–4, p. 439–448, http://dx.doi.org/10.1016/j.geoderma.2008.01.020
Goddéris, Y., Donnadieu, Y., de Vargas, C., Pierrehumbert, R. T., Dromart, G., and van de Schootbrugge, B., 2008b, Causal or casual link between the rise of nannoplankton calcification and a tectonically-driven massive decrease in Late Triassic atmospheric CO_2?: Earth and Planetary Science Letters, v. 267, n. 1–2, p. 247–255, http://dx.doi.org/10.1016/j.epsl.2007.11.051
Goddéris, Y., Donnadieu, Y., Lefebvre, V., Le Hir, G., and Nardin, E., 2012, Tectonic control of continental weathering, atmospheric CO_2, and climate over Phanerozoic times: Comptes Rendus Geoscience, v. 344, p. 652–662, http://dx.doi.org/10.1016/j.crte.2012.08.009
Goddéris, Y., Donnadieu, Y., Le Hir, G., Lefebvre, V., and Nardin, E., 2014, The role of palaeogeography in the Phanerozoic history of atmospheric CO_2 and climate: Earth-Science Reviews, v. 128, p. 122–138, http://dx.doi.org/10.1016/j.earscirev.2013.11.004
Gough, D. O., 1981, Solar interior structure and luminosity variations: Solar Physics, v. 74, n. 1, p. 21–34, http://dx.doi.org/10.1007/BF00151270
Gradstein, F. M., Ogg, J. G., and Smith, A. G., 2004, A Geologic Timescale 2004: Cambridge, Cambridge University Press, 589 p.
Hansen, J., Sato, M., Kharecha, P., Beerling, D., Berner, R., Masson-Delmotte, V., Pagani, M., Raymo, M., Royer, D. L., and Zachos, J. C., 2008, Target atmospheric CO_2: Where should humanity aim?: The Open Atmospheric Science Journal, v. 2, p. 217–231, http://dx.doi.org/10.2174/1874282300802010217
Hayes, J. M., Strauss, H., and Kaufman, A. J., 1999, The abundance of ^{13}C in marine organic matter and isotopic fractionation in the global biogeochemical cycle of carbon during the past 800 Ma: Chemical Geology, v. 161, n. 1–3, p. 103–125, http://dx.doi.org/10.1016/S0009-2541(99)00083-2
IPCC, 2013, Climate Change 2013: The Physical Science Basis, Contribution of Working Group I to the Fifth Assessment Report of the Intergovernmental Panel on Climate Change, Stocker, T. F., Qin, D., Plattner, G.-K., Tignor, M., Allen, S. K., Boschung, J., Nauels, A., Xia, Y., Bex, V., and Midgley, P. M., editors: Cambridge, Cambridge University Press, 1535 p.
Lee, C.-T. A., Shen, B., Slotnick, B. S., Liao, K., Dickens, G. R., Yokoyama, Y., Lenardic, A., Dasgupta, R., Jellinek, M., Lackey, J. S., Schneider, T., and Tice, M. M., 2013, Continental arc–island arc fluctuations, growth of crustal carbonates, and long-term climate change: Geosphere, v. 9, n. 1, p. 21–36, http://dx.doi.org/10.1130/GES00822.1
Lefebvre, V., Donnadieu, Y., Goddéris, Y., Fluteau, F., and Hubert-Théou, L., 2013, Was the Antarctic glaciation delayed by a high degassing rate during the early Cenozoic?: Earth and Planetary Science Letters, v. 371–372, p. 203–211, http://dx.doi.org/10.1016/j.epsl.2013.03.049
Maher, K., and Chamberlain, C. P., 2014, Hydrologic regulation of chemical weathering and the geologic carbon cycle: Science, v. 343, n. 6178, p. 1502–1504, http://dx.doi.org/10.1126/science.1250770
Moulton, K. L., West, J., and Berner, R. A., 2000, Solute flux and mineral mass balance approaches to the quantification of plant effects on silicate weathering: American Journal of Science, v. 300, n. 7, p. 539–570, http://dx.doi.org/10.2475/ajs.300.7.539
Müller, R. D., Dutkiewicz, A., Seton, M., and Gaina, C., 2013, Seawater chemistry driven by supercontinent assembly, breakup, and dispersal: Geology, v. 41, n. 8, p. 907–910, http://dx.doi.org/10.1130/G34405.1
Nardin, E., Goddéris, Y., Donnadieu, Y., Hir, G. L., Blakey, R. C., Pucéat, E., and Aretz, M., 2011, Modeling the early Paleozoic long-term climatic trend: Geological Society of America Bulletin, v. 123, n. 5–6, p. 1181–1192, http://dx.doi.org/10.1130/B30364.1
Otto-Bliesner, B. L., 1995, Continental drift, runoff and weathering feedbacks: Implications from climate model experiments: Journal of Geophysical Research, v. 100, n. D6, p. 11537–11548, http://dx.doi.org/10.1029/95JD00591
Pagani, M., Liu, Z., LaRiviere, J., and Ravelo, A. C., 2010, High Earth-system climate sensitivity determined from Pliocene carbon dioxide concentrations: Nature Geoscience, v. 3, p. 27–30, http://dx.doi.org/10.1038/ngeo724
Park, J., and Royer, D. L., 2011, Geologic constraints on the glacial amplification of Phanerozoic climate sensitivity: American Journal of Science, v. 311, n. 1, p. 1–26, http://dx.doi.org/10.2475/01.2011.01
Price, G. D., Twitchett, R. J., Wheeley, J. R., and Buono, G., 2013, Isotopic evidence for long term warmth in the Mesozoic: Scientific Reports, v. 3, 1438, http://dx.doi.org/10.1038/srep01438
Prokoph, A., Shields, G. A., and Veizer, J., 2008, Compilation and time-series analysis of a marine carbonate $\delta^{18}O$, $\delta^{13}C$, and $^{87}Sr/^{86}Sr$ and $\delta^{34}S$ database through Earth history: Earth-Science Reviews, v. 87, n. 3–4, p. 113–133, http://dx.doi.org/10.1016/j.earscirev.2007.12.003

R Core Team, 2014, R: A Language and Environment for Statistical Computing: Vienna, Austria, R Foundation for Statistical Computing. http://www.r-project.org/

Roe, G. H., and Baker, M. B., 2007, Why is climate sensitivity so unpredictable?: Science, v. 318, n. 5850, p. 629–632, http://dx.doi.org/10.1126/science.1144735

Rohling, E. J., Sluijs, A., Dijkstra, H., Köhler, P., van de Wal, R. S. W., von der Heydt, A. S., Beerling, D. J., Berger, A., Bijl, P. K., Crucifix, M., DeConto, R., Drijfhout, S. S., Fedorov, A., Foster, G. L., Ganopolski, A., Hansen, J., Hönisch, B., Hooghiemstra, H., Huber, M., Huybers, P., Knutti, R., Lea, D. W., Lourens, L. J., Lunt, D., Masson-Demotte, V., Medina-Elizalde, M., Otto-Bliesner, B., Pagani, M., Pälike, H., Renssen, H., Royer, D. L., Siddall, M., Valdes, P., Zachos, J. C., and Zeebe, R. E., 2012, Making sense of palaeoclimate sensitivity: Nature, v. 491, p. 683–691, http://dx.doi.org/10.1038/nature11574

Rowley, D. B., 2002, Rate of plate creation and destruction: 180 Ma to present: Geological Society of America Bulletin, v. 114, n. 8, p. 927–933, http://dx.doi.org/10.1130/0016-7606(2002)114<0927:ROPCAD>2.0.CO;2

Royer, D. L., 2014, Atmospheric CO_2 and O_2 during the Phanerozoic: tools, patterns, and impacts, *in* Farquhar, J., editor, The Atmosphere-History: Oxford, Elsevier, Treatise on Geochemistry (Second Edition), v. 6, p. 251–267, http://dx.doi.org/10.1016/B978-0-08-095975-7.01311-5

Royer, D. L., Berner, R. A., and Park, J., 2007, Climate sensitivity constrained by CO_2 concentrations over the past 420 million years: Nature, v. 446, p. 530–532, http://dx.doi.org/10.1038/nature05699

Royer, D. L., Pagani, M., and Beerling, D. J., 2012, Geobiological constraints on Earth system sensitivity to CO_2 during the Cretaceous and Cenozoic: Geobiology, v. 10, n. 4, p. 298–310, http://dx.doi.org/10.1111/j.1472-4669.2012.00320.x

Scott, A. C., and Glasspool, I. J., 2006, The diversification of Paleozoic fire systems and fluctuations in atmospheric oxygen concentration: Proceedings of the National Academy of Sciences of the United States of America, v. 103, n. 29, p. 10861–10865, http://dx.doi.org/10.1073/pnas.0604090103

Urey, H. C., 1952, The Planets: Their Origin and Development: New Haven, Yale University Press, 245 p.

van der Meer, D., Zeebe, R. E., van Hinsbergen, D. J. J., Sluijs, A., Spakman, W., and Torsvik, T. H., 2014, Plate tectonic controls on atmospheric CO_2 levels since the Triassic: Proceedings of the National Academy of Sciences of the United States of America, v. 111, n. 12, p. 4380–4385, http://dx.doi.org/10.1073/pnas.1315657111

Vaughan, A. P. M., 2007, Climate and geology - a Phanerozoic perspective, *in* Williams, M., Haywood, A. M., Gregory, F. J., and Schmidt, D. N., editors, Deep-Time Perspectives on Climate Change: Marrying the Signal from Computer Models and Biological Proxies: London, The Geological Society and The Micropalaeontological Society, Special Publications, p. 5–59, http://nora.nerc.ac.uk/id/eprint/4237

Walker, J. C. G., Hays, P. B., and Kasting, J. F., 1981, A negative feedback mechanism for the long-term stabilization of Earth's surface temperature: Journal of Geophysical Research-Oceans, v. 86, n. C10, p. 9776–9782, http://dx.doi.org/10.1029/JC086iC10p09776

Ward, J. K., Harris, J. M., Cerling, T. E., Wiedenhoeft, A., Lott, M. J., Dearing, M.-D., Coltrain, J. B., and Ehleringer, J. R., 2005, Carbon starvation in glacial trees recovered from the La Brea tar pits, southern California: Proceedings of the National Academy of Sciences of the United States of America, v. 102, p. 690–694, http://dx.doi.org/10.1073/pnas.0408315102

Wildman, R. A., Jr., Hickey, L. J., Dickinson, M. B., Berner, R. A., Robinson, J. M., Dietrich, M., Essenhigh, R. H., and Wildman, C. B., 2004, Burning of forest materials under late Paleozoic high atmospheric oxygen levels: Geology, v. 32, n. 5, p. 457–440, http://dx.doi.org/10.1130/G20255.1

Wilkinson, B. H., and Walker, J. C. G., 1989, Phanerozoic cycling of sedimentary carbonate: American Journal of Science, v. 289, n. 4, p. 525–548, http://dx.doi.org/10.2475/ajs.289.4.525

Wu, N., Farquhar, J., Strauss, H., Kim, S.-T., and Canfield, D. E., 2010, Evaluating the S-isotope fractionation associated with Phanerozoic pyrite burial: Geochimica et Cosmochimica Acta, v. 74, n. 7, p. 2053–2071, http://dx.doi.org/10.1016/j.gca.2009.12.012